NASA Contractor Report 3877

Stress Waves in an Isotropic Elastic Plate Excited by a Circular Transducer

Hira Karagulle, James H. Williams, Jr., and Samson S. Lee

NASA

NASA Contractor Report 3877

Stress Waves in an Isotropic Elastic Plate Excited by a Circular Transducer

Hira Karagulle, James H. Williams, Jr., and Samson S. Lee

Massachusetts Institute of Technology
Cambridge, Massachusetts

NASA

National Aeronautics
and Space Administration

Scientific and Technical
Information Branch

1985

ABSTRACT

Steady-state harmonic stress waves in an isotropic elastic plate excited on one face by a circular transducer are analyzed theoretically. It is assumed that the transmitting transducer transforms an electrical voltage into a uniform normal stress at the top face of the plate. To solve the boundary value problem, first the radiation into a half- space is considered. This introduces longitudinal (P) and shear (S) waves into the plate. Then, reflections are considered successively at the bottom and top faces of the plate. Each reflection produces both P and S waves for each incident P or S wave.

A separate circular receiving transducer, also located at the top face of the plate, is considered. It is assumed that the receiving transducer produces an electrical voltage proportional to the average spatially integrated normal stress over its face due to an incident wave.

The asymptotic behavior of the frequency response at a receiving point due to a multiply reflected wave is given. It is found that a receiving point observes an incident wave asymptotically as a plane wave which propogates and reflects in the direction of the multiply reflected ray constructed geometrically using Snell's law. The far field condition, for which the asymptotic solution is valid, is also discussed. This condition suggests that although the thickness of the plate may be small, the waves which reflect sufficiently many times do satisfy the far field condition.

A numerical procedure is given to evaluate the frequency response at a receiving point due to a multiply reflected wave in the near field. Its stability and convergence are discussed. Also, exponential decay is introduced

to account for material attenuation.

Calculations are done for aluminum plates. It is found that the numerical procedure becomes unstable for $h/\lambda_1 < 1.6$ where h is the thickness of the plate and λ_1 is the P wavelength.

Parametrized plots which determine the particular wave whose frequency response has maximum magnitude compared with other multiply reflected waves are given for a range of values of dimensionless parameters. The effects of changes in the values of the parameters are discussed.

1 INTRODUCTION

An ultrasonic testing (UT) parameter called the stress wave factor (SWF) was recently introduced by Vary et al. [1,2] for nondestructive evaluation (NDE) of materials. In the SWF configuration, separate transmitting and receiving transducers are coupled to the same face of the test structure and the number of oscillations exceeding a preselected voltage threshold (or some modifications thereof [3]) in the output signal, due to an input pulse having a broadband frequency spectrum, is defined as the stress wave factor. Williams and Lampert [3] indicated a correlation between the SWF and the attenuation in carbon fiber composites by showing that as the residual strength decreases due to impact damage, the SWF decreases and the through- transmission ultrasonic attenuation increases. Williams et al. have also shown that the initial through- transmission longitudinal attenuation can be correlated with the compression fatigue life [4] and the flexural fatigue life [5] of carbon fiber composites.

Unlike conventional pulse- echo testing [6] where nonoverlapping reflected wave echoes are analyzed, the SWF is also valid for the analysis of overlapping echoes.

Although the SWF has been generally used to characterize microstructural defect states of materials, it may also be used to detect cracks and delaminations by coupling separate transmitting and receiving transducers to the same face of the test structure. The output in such a SWF configuration may be significantly affected by cracks oriented perpendicular to the faces of the structure, which are otherwise difficult to detect by most NDE methods.

An important step in any quantitative ultrasonic NDE procedure is the

analysis of the stress wave transmission chracteristics of the test structure through which the transmitting and receiving transducers communicate. The ultrasonic input- output characteristics of the SWF configuration containing thick isotropic elastic plates are studied in [7] theoretically and experimentally. It is assumed that the transmitting transducer transforms an electrical voltage into a uniform normal stress on the plate and vice versa for the receiving transducer. The asymptotic value of the normal stress is calculated for an isotropic elastic half- space subjected to a uniform harmonic normal stress applied to a circular region at its surface, using the results of Miller and Pursey [8]. The top surface of the plate is assumed to coincide with the surface of the half- space and the bottom surface of the plate is assumed to be at a depth within the half- space equal to the plate thickness. Then the radiated stress waves are traced within the plate by considering reflections at its top and bottom faces. Reflection coefficients for plane waves are used assuming that the thickness of the plate is so large that the bottom face of the plate is in the far field of the transmitting transducer and the asymptotic spherical waves are nearly plane at the point of reflection.

The purpose of this study is to extend the analysis for thick plates given in [7] to plates of any thicknesses; in particular, to plates whose thicknesses are smaller than the far field distance of the transmitting transducer.

One way to address the boundary conditions which are imposed by the transmitting transducer at the top face and the boundary conditions at the stress- free bottom face is to expand the radially propagating plate waves which are derived by the nonlinear Rayleigh- Lamb frequency spectrum [9]. Such

an approach would be especially useful at low frequencies where the thickness of the plate is of the order of the longitudinal wavelength because a small number of radially propagating waves would be excited.

Another way to approach the problem, which is more practical at high frequencies where the thickness of the plate is much larger than the longitudinal wavelength, is to consider the radiation from the transmitting transducer into a half- space and then to introduce succesive multiply reflected waves at the bottom and top faces of the plate. Each multiply reflected wave whose potential is expressed in integral form is called a generalized ray. This method is often called the generalized ray theory and is discussed in [10]. Transient waves generated by a variety of internal and surface forces in a plate have been analyzed by Pao and Gajewski [10], and Ceranoglu and Pao [11] using this approach.

2 STRESS WAVES IN THE PLATE

2.1 Governing Equations and Boundary Conditions

Consider an isotropic elastic plate of thickness h, bounded by the z=0 and z=h planes and extending infinitely in the x and y directions as shown in Fig. 1 (a). As done in [7], it is assumed that the transmitting transducer transforms an electrical voltage into a uniform normal stress on the plate. The cartesian coordinates x,y,z; the cylindrical coordinates r,$\varnothing$,z; and the spherical coordinates R,Θ,$\varnothing$ are shown in Fig. 1 (b).

Then, the boundary conditions on the top face of the plate, including those imposed by the transmitting transducer, for steady-state conditions can be written as

at z=0 :

$$\sigma_{zz} = \begin{cases} e^{-i\omega t} & \text{for} \quad 0 \leq r \leq a_1 \\ 0 & \text{for} \quad r > a_1 \end{cases} \qquad (1)$$

$$\sigma_{rz} = \sigma_{z\varnothing} = 0$$

where σ_{zz}, σ_{rz}, $\sigma_{z\varnothing}$ are the components of the stress tensor in the cylindrical coordinates [12], ω is radian frequency, t is time, $i \equiv \sqrt{-1}$, and a_1 is the radius of the transmitting transducer. The amplitude of σ_{zz} is taken as the unity since only the frequency response of the plate is of interest. Because the bottom face of the plate is stress- free, the boundary conditions there can be stated as

at z=h :

$$\sigma_{zz} = \sigma_{rz} = \sigma_{z\mathscr{O}} = 0 \qquad\qquad (2)$$

Because of the circularity of the excitation, there is axial symmetry about the z axis and so the displacement component in the $\mathscr{O}$ direction vanishes. Then, the theory of wave propogation suggests that the following uncoupled wave equations are satisfied within an isotropic elastic solid [12]

$$\nabla^2\Phi = \frac{1}{c_1^2}\frac{\partial^2\Phi}{\partial t^2} \qquad\qquad (3)$$

$$\nabla^2\Psi = \frac{1}{c_2^2}\frac{\partial^2\Psi}{\partial t^2} \qquad\qquad (4)$$

where ∇^2 is the laplacian operator and for cylindrical coordinates with axial symmetry is given by

$$\nabla^2 = \frac{\partial^2}{\partial r^2} + \frac{1}{r}\frac{\partial}{\partial r} + \frac{\partial^2}{\partial z^2} \qquad\qquad (5)$$

Φ and Ψ are uncoupled longitudinal (P) and shear (S) wave potentials; and c_1 and c_2 are the P and S wave velocities, respectively. The components of the displacement and stress fields can be found from the potentials and the relations are summarized in Table 1.

The complete solution requires finding the wave potentials which satisfy

either eqn. (3) or eqn. (4) such that the superpositions of the stresses generated from these potentials via the relations given in Table 1 satisfy the boundary conditions at z=0 and z=h as given by eqns. (1) and (2), respectively.

2.2 Half-space Solution

At the first stage of the solution, the boundary conditions at z=h are ignored. Then the problem reduces to that of radiation into a half- space. Using Hankel transform techniques, Miller and Pursey [8] solved this problem for the boundary conditions given in eqn. (1). That solution is reviewed in [13] with the notation used in this study and is given by

$$\Phi_P = \frac{2\pi a_1}{\mu\lambda_1} \int_0^\infty E_P(\xi)\, J_0(2\pi\xi\frac{r}{\lambda_1})\, \exp(2\pi i\frac{z}{\lambda_1}\sqrt{1-\xi^2})\, d\xi \qquad (6)$$

and

$$\Phi_S = \frac{2\pi a_1}{\mu\lambda_1} \int_0^\infty E_S(\xi)\, J_0(2\pi\xi\frac{r}{\lambda_1})\, \exp(2\pi i\frac{z}{\lambda_1}\sqrt{k^2-\xi^2})\, d\xi \qquad (7)$$

where Φ_P and Φ_S are the P and S wave potentials which satisfy eqns. (3) and (4), respectively. The shear modulus of the plate material is μ; λ_1 is the P wavelength and is given by $\lambda_1 = 2\pi c_1/\omega$; ξ is a dimensionless integration variable introduced in the Hankel transform; J_0 denotes a Bessel function of the first kind and of order zero; $k=c_1/c_2$; $E_P(\xi)$ and $E_S(\xi)$ are called the excitation functions for the P and S waves, respectively, and are given by

$$E_P(\xi) = \frac{(2\xi^2 - k^2)}{G(\xi)} J_1(2\pi\xi\frac{a_1}{\lambda_1}) \qquad (8)$$

$$E_S(\xi) = -2i \frac{\sqrt{1-\xi^2}}{G(\xi)} J_1(2\pi\xi\frac{a_1}{\lambda_1}) \qquad (9)$$

where

$$G(\xi) = (2\xi^2 - k^2)^2 + 4\xi^2 \sqrt{1-\xi^2} \sqrt{k^2 - \xi^2} \qquad (10)$$

and J_1 is a Bessel function of the first kind and of order one.

The potentials given in eqns. (6) and (7) and the potentials which are introduced below all have a steady- state harmonic time dependence, indicated by $\exp(-i\omega t)$; this harmonic time dependence function is dropped from the expressions for convenience.

The excitation functions in eqns. (8) and (9) have a pole at $\xi = \xi_R$ where the denominator function, $G(\xi)$, given in eqn. (10) vanishes when $\xi_R = c_R/c_1$ where c_R is the Rayleigh wave velocity. ξ_R is the so- called Rayleigh pole.

2.3 Reflected Waves

The superpositions of the stresses generated from the potentials Φ_P and Φ_S satisfy the boundary conditions at z=0 only. So, in the so- called first stage the boundary conditions at z=h are violated. In the second stage, new waves which are called reflected waves are introduced so that the boundary conditions at z=h are then satisfied. This requires introducing a set of P and S waves for each P and each S wave initiated in the first stage, which is due to mode conversion [14]. These new waves are called the PP and PS, and SP and SS waves and their potentials are denoted by Φ_{PP} and Φ_{PS}, and Φ_{SP} and Φ_{SS},

respectively. In particular the potentials Φ_{PP} and Φ_{PS} are introduced to cancel the stresses σ_{zz} and σ_{rz} at z=h generated from the potential Φ_P, corresponding to the reflection of the P wave at the stress- free plane boundary at z=h.

The superpositions of the stresses generated from the potentials introduced in the first and second stages satisfy the boundary conditions at z=h only. In the third stage, additional reflected waves are introduced so that the boundary conditions at z=0 are then satisfied. Again, this requires introducing a set of P and S waves for each P and each S wave introduced in the second stage and they are called the PPP and PPS, and PSP and PSS, ..., for a total of eight. In particular the potentials of the SPP and SPS waves, Φ_{SPP} and Φ_{SPS}, respectively, are introduced at z=0 to cancel the stresses σ_{zz} and σ_{rz} generated from the potential Φ_{SP}, corresponding to the reflection of the SP wave at a stress- free plane boundary at z=0.

The superpositions of the stresses generated from the potentials introduced in the first, second and third stages satisfy the boundary conditions at z=0 only. The procedure of adding new reflected waves at each successive stage can be continued as above. At each stage, a new set of P and S waves for each P and each S wave introduced at the previous stage is added. This process is represented in Fig. 2 as a binary tree. At each stage, the boundary conditions at one face are satisfied and the boundary conditions at the other face are destroyed. However, as shown below, the waves introduced for increasingly large numbers of stages, namely the waves with very large numbers of reflections, vanish. Thus, the superpositions of all the stresses generated from the wave potentials from the first stage to infinity satisfy the boundary conditions at both z=0 and z=h simultaneously. Also, again as

shown below, the waves with increasingly higher numbers of reflections are observed at a receiving point with increasingly larger time delays; and thus considering a finite number of waves is sufficient for the exact analysis of a transient response up to a fixed time.

In studying the wave propogation in a multi- layered elastic medium, Spencer [14] analyzed multiple reflections and transmissions of axially symmetric waves at plane boundaries. Following the analysis given in [14], in general the potential of a particular wave which has a unique chain of P's and S's can be shown to be [13]

$$\Phi_{n/j} = \frac{2\pi a_1}{\lambda_1} \int_0^\infty E(\xi) \, Q(\xi) \, J_0(2\pi\xi\frac{r}{\lambda_1}) \, \exp\{2\pi i[\frac{h}{\lambda_1}((p-m_1)\sqrt{1-\xi^2}$$

$$+(s-m_2)\sqrt{k^2-\xi^2})+m\frac{z}{\lambda_1}\sqrt{b^2-\xi^2}]\} \, d\xi \qquad (11)$$

where $\Phi_{n/j}$ denotes the particular wave potential and is called the j-th wave potential at the n-th stage. The unique chain for the particular wave potential is found by converting the decimal integer j to the corresponding n bit binary number and then assigning P's for 0's and S's for 1's in the binary number. n can take values from 1 to ∞, and j can take values from 0 to 2^n-1. For example, the chain for the wave whose potential is represented by $\Phi_{4/5}$ can be found as follows. First, j=5 is converted to the n=4 bit binary number 0101, and then P's for 0's and S's for 1's are assigned in the binary number, which results in the PSPS wave.

E(ξ) in eqn. (11) is called the excitation function and is equal to $E_P(\xi)$ or $E_S(\xi)$ if $\Phi_{n/j}$ is constructed from the half-space solution Φ_P or Φ_S

(that is, if the chain for $\Phi_{n/j}$ started with a P or an S wave), respectively. $Q(\xi)$ is called the product of the reflection coefficients and is given below. The numbers p and s represent the total number of P's and S's in the chain, respectively, and n=p+s. m_1 is equal to 1 if the last reflection occurs at z=0 (that is, if n is odd) and if $\Phi_{n/j}$ is a P wave potential (that is if the chain ends with P). Otherwise m_1 is zero. m_2 is equal to 1 if n is odd and if $\Phi_{n/j}$ is an S wave potential (that is, if the chain ends with S). Otherwise m_2 is zero. m is equal to +1 or -1 if the last reflection occurs at z=0 or z=h (that is, if n is odd or even), respectively. b is equal to 1 or k if $\Phi_{n/j}$ is a P or S wave potential (that is, if the chain ends with P or S, or equivalently if j is even or odd), respectively.

The product of reflection coefficients is given by

$$Q(\xi) = [Q_{PP}(\xi)]^{j_1} \, [\frac{-i}{\xi} Q_{PS}(\xi)]^{j_2} \, [i\xi Q_{SP}(\xi)]^{j_3}$$

$$[Q_{SS}(\xi)]^{j_4} \, (-1)^{j_5+j_6} \qquad (12)$$

where j_1, j_2, j_3, and j_4 are the total number of P to P, P to S, S to P, and S to S reflections, respectively; and j_5 and j_6 are the total number of P to S and S to P reflections only at z=h, respectively. Q_{PP}, Q_{PS}, Q_{SP}, and Q_{SS} are the P to P, P to S, S to P, and S to S reflection coefficients, respectively, and are given by

$$Q_{PP}(\xi) = Q_{SS}(\xi) = \frac{4\xi^2 \sqrt{1-\xi^2} \sqrt{k^2-\xi^2} - (2\xi^2-k^2)^2}{G(\xi)} \qquad (13)$$

$$Q_{PS}(\xi) = \frac{4\xi \sqrt{1-\xi^2} (k^2-2\xi^2)}{G(\xi)} \qquad (14)$$

$$Q_{SP}(\xi) = \frac{-4\xi \sqrt{k^2-\xi^2} (k^2-2\xi^2)}{G(\xi)} \qquad (15)$$

j_1, j_2, j_3, j_4, j_5, and j_6 can be found from the specific wave chain. For example for the PPSSPS wave, they are 1, 2, 1, 1, 1, and 0, respectively. Also for this particular wave $E(\xi)=E_P(\xi)$; $p=3$ and $s=3$; $m_1=0$ and $m_2=0$; $m=-1$ and $b=k$.

So, as discussed above the superpositions of the stresses generated from the potentials introduced in the first stage as the half-space solution and all the possible reflected wave potentials introduced in the successive stages satisfy the boundary conditions at both $z=0$ and $z=h$ as given by eqns. (1) and (2), respectively.

3 FREQUENCY RESPONSE OF THE PLATE

In general, a receiving transducer located on the plate observes a physical quantity such as stress, strain, or displacement generated from incident wave potentials. In this study, the SWF configuration is considered and it is assumed that a circular receiving transducer, which is separate from the transmitting transducer, is located at the top face of the plate. As in [7], it is assumed that the receiving transducer produces an electrical voltage proportional to the normal stress, σ_{zz}, generated from an incident wave potential averaged over its contact area. The receiving transducer therefore observes only the reflected waves at z=h which are introduced at the even numbered stages.

It should be noted that the existence of the receiving transducer is not taken into consideration in Sec. 2, where stress waves in the plate are studied. Then, the question arises as to whether or not the receiving transducer affects the waves in the plate at the point of reception. The waves in the plate are affected by the presence of the receiving transducer after they reach the receiving transducer. Thus, incident waves on the receiving transducer are not affected, but waves that reflect at the receiving transducer contact area and continue to travel are affected because stress-free boundary conditions are not satisfied on the receiving transducer contact area. In this study, only the incident waves on the receiving transducer are considered and thus the results in Sec. 2 are used.

Since a steady-state harmonic excitation having the magnitude of unity is considered and the plate is assumed to be linear and time invariant, the quantity observed by the receiving transducer may be called the frequency

response of the plate, or simply the frequency response. The quantity observed at a point on the receiving transducer contact area is called the frequency response at a point and is given by

$$H = \sum_{n=2, j=0}^{n=\infty, j=J} H_{n/j} \qquad n=2,4,6,\ldots; \quad J=2^n-1 \qquad (16)$$

where $H_{n/j}$ is the frequency response at a point due to the j-th wave at the n-th stage. After dropping the steady- state term $\exp(-i\omega t)$, $H_{n/j}$ is equal to the normal stress σ_{zz} generated from the wave potential $\Phi_{n/j}$ by the relations given in Table 1 and evaluated at the receiving point at z=0. It is given by [13]

$$H_{n/j} = 2\pi \frac{a_1}{\lambda_1} \int_0^\infty E(\xi) \, Q(\xi) \, V(\xi) \, J_0(2\pi\xi\frac{r}{\lambda_1}) \, \exp[2\pi i\frac{h}{\lambda_1}(p\sqrt{1-\xi^2}$$

$$+s \sqrt{k^2-\xi^2}) \, d\xi \qquad (17)$$

where $V(\xi)$ is called the response function and is equal to the response functions for the P wave $V_p(\xi)$, or for the S wave $V_s(\xi)$ if the potential $\Phi_{n/j}$ is a P or S wave potential, respectively, and where

$$V_p(\xi) = 2\xi^2 - k^2 \qquad (18)$$

$$V_s(\xi) = -2i\xi^2 \sqrt{k^2-\xi^2} \qquad (19)$$

Only even values of n must be considered in eqn. (17) and all subsequent equations in this paper.

The frequency response of the plate, $\bar{H}$, or the frequency response of the plate due to the j-th wave at the n-th stage, $\bar{H}_{n/j}$, can be found by averaging H or $H_{n/j}$, respectively, over the contact area of the receiving transducer. For a receiving transducer of radius a_2, it can be shown that [13]

$$\bar{H}_{n/j} = \frac{2}{\pi a_2^2} \int_{\ell-a_2}^{\ell+a_2} H_{n/j} \; r \; \propto(r) \; dr \qquad (20)$$

where

$$\propto(r) = \tan^{-1} \left\{ \frac{[r^2(2\ell^2+2a_2^2-r^2)-(\ell^2-a_2^2)^2]^{1/2}}{r^2-a_2^2+\ell^2} \right\} \qquad (21)$$

and ℓ is the distance between the transmitting and receiving transducer axes.

The integrals in eqns. (17) and (20) cannot be evaluated analytically in closed form. Thus they are evaluated approximately as discussed in the following sections.

4 ASYMPTOTIC EVALUATION

The integral in eqn. (17) can be evaluated asymptotically by the method of stationary phase [15]. Accordingly, the following can be derived [13]

$$
H_{n/j} \approx -2\pi i \frac{a_1}{\lambda_1} \frac{E(\xi_0)\, Q(\xi_0)\, V(\xi_0)}{\sqrt{(r/\lambda_1)\, \xi_0\, |g''(\xi_0)|}} e^{ig(\xi_0)} \tag{22}
$$

where ξ_0 is the stationary point and which is defined explicitly below. $g(\xi)$ is the phase function and is given by

$$
g(\xi) = 2\pi \frac{h}{\lambda_1} (p\sqrt{1-\xi^2} + s\sqrt{k^2-\xi^2}) + 2\pi \frac{r}{\lambda_1}\xi \tag{23}
$$

| | denotes the "magnitude of" and $g''(\xi)$ is the second derivative of $g(\xi)$ and is given by

$$
g''(\xi) = \frac{d^2 g}{d\xi^2} = \frac{-h}{\lambda_1}\left[\frac{p}{(1-\xi^2)^{3/2}} + \frac{s}{(k^2-\xi^2)^{3/2}}\right] \tag{24}
$$

The first derivative of the phase function vanishes at the stationary point, requiring that the stationary point satisfies the following nonlinear equation

$$
\frac{p\xi_0}{\sqrt{1-\xi_0^2}} + \frac{s\xi_0}{\sqrt{k^2-\xi_0^2}} = \frac{r}{h} \tag{25}
$$

For the interpretation of the equations above, the multiply reflected ray corresponding to the PSSP wave is constructed geometrically between the origin O and a receiving point M in Fig. 3 (a) as an example. A P ray emanating from the origin at an angle Θ_1 reflects as an S ray at N_1, then as an S ray at N_2 and finally as a P ray at N_3 and then propagates to M. Reflection angles are determined by Snell's law [12] and thus all the P and S rays have reflection angles of Θ_1 and Θ_2, respectively, and are related by

$$\sin \Theta_1 = k \sin \Theta_2 \qquad (26)$$

Using the ray geometry and eqn. (26), it can be shown that

$$\xi_0 = \sin \Theta_1 = k \sin \Theta_2 \qquad (27)$$

For unmixed waves, namely for either p=0 or q=0, ξ_0 in eqn. (25) can be evaluated by substituting eqn. (27) into eqn. (25) and using trigonometric functions. Otherwise, numerical techniques such as the method of bisection [16] can be used.

Further, it can be shown that the total distances travelled by the waves as P and S rays, R_1 and R_2, respectively, are given by

$$R_1 = \frac{ph}{\sqrt{1-\xi_0^2}} \qquad (28)$$

$$R_2 = \frac{skh}{\sqrt{k^2-\xi_0^2}} \qquad (29)$$

and the corresponding time delay is given by

$$t_{p,s} = \frac{R_1}{c_1} + \frac{R_2}{c_2} = \frac{g(\xi_0)}{\omega} \qquad (30)$$

Notice that the waves with common p and s, simply the waves with p,s, have the same time delay and the time delay appears as the linearity constant in the phase function which linearly depends on frequency. For example the waves with p=3, s=1 are the PPPS, PPSP, PSPP, and SPPP waves. The frequency response at a point due to the waves with p,s, which is denoted by $\bar{H}_{p,s}$, can be found simply by the superposition of the corresponding frequency responses. The frequency response of the plate due to the waves with p,s, $H_{p,s}$, is then the average $H_{p,s}$ over the contact area of the receiving transducer and can be found similarly by eqn. (20).

Also, it can be shown that the reflection coefficients given by eqns. (13), (14), and (15) are equal to the corresponding reflection coefficients for plane waves [12] when they are evaluated at the stationary point given by eqn. (27). This suggests that a receiving point observes an incident wave asymptotically as a plane wave propogating and reflecting at the bottom and top faces of the plate in the ray directions as constructed above.

The denominator function in eqn. (22) indicates geometrical attenuation for a given combination of r,h,p, and s. It can be visualized by considering a hypothetical multi- layered half-space as shown in Fig. 3 (b). It is assumed that the layers which are identical to the original plate under study and are bonded together in a hypothetical way such that an incident wave in one layer produces no reflected waves but produces transmitted longitudinal and shear waves in the next layer and the transmission coefficients are the same as the reflection coefficients as if the incident wave reflects at a stress- free plane boundary. At the n-th layer in such a medium, only the waves introduced at the n-th stage in the binary tree in Fig. 2 could exsist. The top layer can be thought of as the original plate and each subsequent layer can be thought of as the image of the layer immediately above it. A receiving point M in the original plate and the images of it M_2, M_4, M_6, ... are shown in Fig. 3 (b) The PSSP ray between the origin and M_4 is also shown. So, the geometrical attenuation in eqn. (22) can be observed as due to the spreading of the waves with the distance from the source, and wave mode conversions during transmissions at the boundaries of layers. It can be shown that for unmixed waves, eqn.(22) represents a spherical wave whose magnitude is a function of directivity and decreases with the reflection coefficient $Q_{PP}(\xi_0)=Q_{SS}(\xi_0)$ each time it passes a layer, and the results obtained in [7] can be recovered.

As observed from Fig. 3 (b) qualitatively, although some image points may be in the near field of the source, at sufficiently large distances from the source there are always image points in the far field. The value of the frequency response at a point as given in eqn. (22) is approximately valid for points in the far field.

It should be noted here that in the limit as r approaches zero,

$J_1(2\pi \xi_0 a_1/\lambda_1)/\sqrt{r\xi_0}$ approaches $\pi a_1/(\lambda_1\sqrt{nh})$, and thus eqn. (22) is finite for $r=0$. Also, it can be shown that in the limit as n goes to infinity, $H_{n/j}$ in eqn. (22) goes to zero.

4.1 Near Field and Far Field

The analogy to the acoustics problem considered in [7] is extended to obtain a condition for the asymptotic evaluation in eqn. (22) to be a valid approximation to eqn. (17). The pertinent acoustics problem is that of a rigid piston vibrating in a rigid baffle. The exact formulation in integral form and the asymptotic solution for this problem are given in [17]. They are similar to eqn. (17) and (22), respectively, for unmixed waves.

The exact solution for the radiation pressure along the piston axis can be obtained and is given in [18]. The amplitude of the pressure along the axis (z axis in Fig. 1 (a)) fluctuates near the piston and eventually monotonically approaches the asymptotic solution. The near field and far field distances defined for such a problem are reviewed in [7]. The condition for the asymptotic solution to be valid is stated as

$$z\lambda_0/a^2 > K_F(a/\lambda_0, E_a) \qquad (31)$$

where z is the distance between the origin and the receiving point on the piston axis; λ_0 is the wavelength in the acoustic medium; a is the radius of the piston; and K_F is the far field distance constant which depends on the dimensionless parameters, a/λ_0, and an acceptable error, E_a. E_a is defined as the error between the asymptotic pressure amplitude P_{as} and the exact pressure

amplitude P_{ex} relative to P_{ex}

$$E_a = (P_{as} - P_{ex}) / P_{ex} \qquad (32)$$

Calculated values of K_F for a range of its independent variables are given in Table 2. Notice that for fixed error, K_F becomes constant for a/λ_0 much larger than 1. Also the error decreases with increasing K_F for fixed a/λ_0.

The condition for eqn. (22) to be valid for unmixed waves can be stated by analogy to the acoustics problem. $z\lambda_0/a^2$ in eqn. (31) is replaced by $R_1\lambda_1/a_1^2$ or $R_2\lambda_2/a_1^2$ and the value of K_F for specific values of a_1/λ_1 or a_1/λ_2 and E_a is taken from Table 2. λ_2 is the S wavelength and is equal to λ_1/k.

For mixed waves, the analogy may be extended in a way, which also covers the condition for unmixed waves as special cases. Let the condition be

$$(R_1\lambda_1 + R_2\lambda_2)/a_1^2 > K_F(a_1/\lambda_{av}, E_a) \qquad (33)$$

where λ_{av} is the average wavelength defined by

$$\lambda_{av} = (p\lambda_1 + s\lambda_2)/(p+s) \qquad (34)$$

5 NUMERICAL EVALUATION

The integral in eqn. (17) can also be evaluated by numerical methods [16]. The integral is in the complex ξ-plane because the integrand has singularities at the branch points $\xi = 1$ and $\xi = k$, and at the Rayleigh pole $\xi = \xi_R$ on the integration path from 0 to ∞ [19]. The pole is of order $n = p + s$ because all the reflection functions given by eqns. (13), (14), and (15) have the Rayleigh pole of order 1 as well as the excitation functions given by eqns. (6) and (7). The introduction of appropriate branch cuts and indentations of the integration path on the real axis near the singular points is discussed in [8]. Consistent with the branch cuts introduced, the principal values of $\sqrt{1-\xi^2}$ and $\sqrt{k^2-\xi^2}$ should be considered. Thus the exponential function in the integrand in eqn. (17) is purely oscillatory for $0 \leq \xi < 1$; the part associated with $\sqrt{1-\xi^2}$ monotonically decays, and the part associated with $\sqrt{k^2-\xi^2}$ is oscillatory for $1 < \xi < k$; and monotonically decays for $\xi > k$.

The integration interval from $\xi = 0$ to ∞ is divided into subintervals and as indicated in Table 3, either the trapezoidal rule or Gauss quadrature [16] is used for each subinterval. The integration is stopped at some large value of $\xi = \xi_k$, where $\xi_k > k$, which is justified by the fact that the integrand is exponentially decaying for $\xi > k$. The trapezoidal rule is chosen because it is the simplest method which works well for oscillatory integrands [16]. The Gauss quadrature is chosen in the vicinity of the singular points because it does not require the evaluation of the integrand at the end points of the interval, thus avoiding evaluations at the singular points.

The convergence and stability of the procedures above depend on the exponential decay for $\xi > k$. As shown below, if the decay is not sufficiently

rapid, the effect of the Rayleigh pole is observed as an instability. Increasing h/λ_1, p, or s increases the rate of the exponential decay, thus improving the convergence and stability; however, increasing p or s also increases the power of the pole, thus promoting instability. Thus, there is a compromise associated with increasing p or s in order to achieve a dominance of the exponential decay over the algebraic instability. For a given set of p and s, there is a minimum h/λ_1, $(h/\lambda_1)_{min}$, below which the procedure above gives unstable results. By examining the exponential decay and using the fact that $\sqrt{\xi^2-1} > \sqrt{\xi^2-k^2}$ for $\xi > k$, it can be shown that for the cases with fixed n=p+s the case with p=0, s=n gives the largest $(h/\lambda_1)_{min}$.

The integration over the receiving transducer contact area as given in eqn. (20) can also be performed numerically using the trapezoidal rule.

6 EFFECT OF LOSSES

So far, it has been assumed that the plate material is perfectly elastic and all energy is conserved during wave propogation as only geometrical attenuation due to spreading and wave mode conversions is present. However, wave propogation in real materials is never entirely conservative as a certain amount of energy loss always occurs during propagation and reflections. The mechanisms of these losses are discussed in [20]. In this study, it is assumed that attenuation is small and the effect of the attenuation can be introduced by multiplying eqn. (17) by $\exp[-(\alpha_1 R_1 + \alpha_2 R_2)]$ where α_1 and α_2 are the frequency dependent attenuation constants for P and S waves, respectively [20]. α_1 and α_2 are material properties and have the units of nepers per centimeter [6].

7 RESULTS AND DISCUSSIONS

The frequency response of the plate in the SWF configuration is formulated as the superposition of the frequency responses due to reflected fields. The response of the plate to an arbitrary pulse is thus the the superposition of the responses due to reflected fields to that same pulse, simply reflections, and can be found by Fourier analysis [21].

The frequency responses due to the fields with common p,s have the same phase which depends linearly on frequency; and thus the corresponding reflections whose superposition is called the reflection with p,s have the same time delay in the transient response. If the plate is sufficiently thick, then the time difference between the time delays of the significant reflections with different p,s may be so large that each significant reflection can be observed in the output separately as in [7]. When the plate becomes thinner, the reflections overlap and it is no longer possible to obtain information about an individual reflection directly in the output. However, it may be possible to do so by using homomorphic signal analysis [13,22].

Information about one reflection is useful because it is a prerequisite to analyzing the entire output quantitatively and also because it may be far easier to interpret the changes in individual reflections due to defect states of the plate. This is especially true if the reflection is in the far field, where a receiving point observes the incident field as a plane wave. Although the thickness of the plate may be small, reflections with large enough p or s satisfy the far field condition given by eqn. (34). So, information in the far field may be obtained from some portion of the output signal.

The frequency response at a point due to the field with p,s $H_{p,s}$ depends on the dimensionless parameters p, s, k, $\alpha_1 \lambda_1$, $\alpha_2 \lambda_2$, a_1/λ_1, h/λ_1, and r/h. The frequency response of the plate due to the field with p,s $\bar{H}_{p,s}$ also depends on the dimensionless parameters p, s, k, $\alpha_1 \lambda_1$, $\alpha_2 \lambda_2$, a_1/λ_1, h/λ_1, ℓ/h, and a_2/a_1. Unless otherwise stated, it is assumed that the plate material is lossless, namely $\alpha_1 = \alpha_2 = 0$, in the following calculations. Also, aluminum for which k=2.02 is considered as the plate material.

The behavior of $|H_{2,0}|$, $|H_{6,0}|$, and $|H_{3,1}|$ versus h/λ_1 is plotted in Figs. 4 (a), (b), and (c), respectively, for the values of a_1/λ_1 of 3 for all cases and for r/h of 0, 0, and 2.5, respectively. The magnitudes calculated using the asymptotic formula in eqn. (23) are indicated by the filled squares. The magnitudes calculated by evaluating the integral in eqn. (18) by the numerical procedures described in Sec. 5 are indicated by solid curves.

The asymptotic magnitude in Fig. 4 (a) shows spherical wave behavior, and thus it starts to "blow up" for small h/λ_1, namely, near to the source. The numerical magnitude has approximately the same value as the asymptotic magnitude for large h/λ_1 (for $h/\lambda_1 > 14.4$ with the criterion given by eqn. (34)) and it is oscillatory for smaller h/λ_1. The numerical magnitude also "blows up" at $(h/\lambda_1)_{min} \approx 0.48$ because of the effect of the Rayleigh pole as discussed in Sec. 5. Similar discussions can be given for Figs. 4 (b) and (c).

As discussed in Sec. 5 $(h/\lambda_1)_{min}$ is controlled by p and s. For the cases with fixed n=p+s, the case with p=0, s=n gives the largest $(h/\lambda_1)_{min}$. $(h/\lambda_1)_{min}$ has been evaluated for the cases with increasing s and fixed p=0, $a_1/\lambda_1 = 3$, r/(sh)=0.7. It increases with increasing s and gives a peak value at aproximately 1.6 for s=10 and then decreases as suggested by the discussions on the stability of the numerical procedure in Sec. 5. The critical h/λ_1,

$(h/\lambda_1)_{cr}$, which is the largest $(h/\lambda_1)_{min}$ among all the cases, is approximately 1.6. $(h/\lambda_1)_{cr}$ limits the applicability of the formulations in this study. For $h/\lambda_1 \langle\langle h/\lambda_1\rangle_{cr}$, expanding the plate modes derived by Rayleigh- Lamb frequency spectrum, which is more suitable for low frequencies, may be used.

Some parametrized plots which determine the particular field whose frequency response has the maximum magnitude compared with other reflected fields are given in Figs. 5-8. These plots may also be used in the spectral analysis of transient signals to estimate the particular reflection which has the maximum magnitude compared with other reflections at a particular frequency. The reflection with the maximum magnitude is important because it has the maximum signal to noise ratio in an experiment.

Since the transmitting and receiving transducers considered in this study are longitudinal, the reflections with only P waves, namely with $s=0$, will be dominant in the output [7,13]; and thus only the fields with $s=0$ are considered. Again, $k=2.02$ is used, but the results can be generated for other materials.

In Fig. 5 (a), a point receiver, namely $a_2/a_1 =0$; a lossless material, namely $\alpha_1\lambda_1 =0$; and $a_1/\lambda_1 =1$ are considered. The abscissa and the ordinate are h/λ_1 and ℓ/a_1, respectively. Then all the parameters in this analysis except p are fixed for each point in the $(h/\lambda_1, \ell/a_1)$ plane.

Suppose the magnitude of the frequency response at a particular point due to the field with $p=p_{max}$ is maximum among all the possible fields with $p=2$ to ∞. p_{max} will be found to be the same for each point in a region bounded by solid curves in Fig. 5 (a) (and is indicated in each region. For example, $p_{max}=4$ for $h/\lambda_1 =6$, $\ell/a_1 =5$.

In generating Figs. 5 8, discrete points where h/λ_1 and ℓ/a_1 change from

2 to 40 and 2 to 10, respectively, with increments of 1 have been considered. Then $|\bar{H}_{p,0}|$ (actually $|H_{p,0}|$ for a point receiver) has been calculated for each point by changing p from 2 to a sufficiently large number, in increments of 2. The asymptotic formula given by eqn. (23) has been used if the condition given by eqn. (34) has been satisfied with the value of K_F for E_a=5% in Table 2. The numerical procedure discussed in Sec. 5 has been used otherwise. $|\bar{H}_{p,0}|$ may have diverged with increasing p at the beginning, but it has finally converged to zero due to geometrical attenuation as discussed in Sec. 4. Thus, the sufficiently large number for p has been set by checking the convergence and when $|\bar{H}_{p,0}|$ has become negligible (20 dB down) compared with the maximum magnitude. The curves dividing the regions having the same p_{max} have been then generated by linear interpolation.

Similar plots are given in Figs. 5 (b) and (c) where only a_1/λ_1 as 3 and 5, respectively, is changed. For the plots in Fig. 6, again lossless material but a_2/a_1=1 are considered, and a_1/λ_1 is 1,3, and 5 for Figs. 6 (a), (b), and (c), respectively. In Fig.7 the conditions are the same as in Fig. 5 (b) except $\alpha_1\lambda_1$ is changed to 0.005 and 0.01 in Figs. 7 (a), and (b), respectively. Similarly, the conditions in Fig. 8 are the same as in Fig. 6 (b) except $\alpha_1\lambda_1$ is changed to 0.005 and 0.01 in Figs. 8 (a) and (b), respectively.

There are several observations which can be made from these plots.

1. In the plots in Fig. 5, all the fields with $p=p_{max}$ are in the far field. p_{max} decreases with increasing h/λ_1 and increases with increasing ℓ/a_1 and a_1/λ_1. As a_1/λ_1 becomes larger or h/λ_1 becomes smaller, changes in h/λ_1 or ℓ/a_1 produce larger changes in p_{max}.

In order to understand these and the following observations, consider

the hypothetical multi- layered half space in Fig. 3 (b) again, and consider only the P waves in the medium. Then the field with only P waves observed at an image point M_p is the field with p,s=0 observed at the receiving point M in the original plate as discussed in Sec. 4. Since the excitation with a_1/λ_1 is longitudinal in the z direction, the field with P waves only dies out at the points located away from the source. As discussed in Sec. 4, in the far field it is a spherical wave whose amplitude is a function of directivity and decreases due to mode conversions each time it passes a layer. The polar diagrams of the directivity function for several a_1/λ_1 are given in [7]. It is mainly controlled by the function $f(u)=|J_1(u)/u|$ where $u=2\pi\xi_0 a_1/\lambda_1$ and $\xi_0=\sin\Theta_1$. The properties of $f(u)$ is discussed in [23]. For sufficiently large a_1/λ_1, the directivity function has a main lobe where it has a maximum at $\Theta_1=0$ and decreases to zero, and beyond which it has successive side lobes where it reaches a maximum and decreases to zero with increasing Θ_1. The maximums in the side lobes decrease with increasing angle Θ_1 and they are much smaller than the maximum at $\Theta_1=0$. The number of side lobes increases with increasing a_1/λ_1 and the main lobe is confined to a smaller angle. Thus, the decrease in the directivity function with increasing angle becomes faster. For small a_1/λ_1, the directivity function has only a main lobe and it never becomes zero.

Now notice that an image point M_p in Fig. 3 (b) is located at a larger distance R_1 but at a smaller angle Θ_1 with increasing p. Then $|\bar{H}_{p,0}|$ tends to decrease due to larger geometrical attenuation because of the larger distance and larger number of mode conversions, but also it tends to increase due to the directivity function because of the smaller angle with increasing p. So, there is a compromise in the value of p_{max}.

As h/λ_1 increases or ℓ/a_1 decreases Θ_1 becomes smaller for smaller p and p_{max} tends to decrease because of the directivity function. As a_1/λ_1 increases the value of the directivity function for larger Θ_1, namely for smaller p, becomes smaller and p_{max} tends to increase. For smaller h/λ_1, changes in h/λ_1 or ℓ/a_1 produce larger changes in Θ_1 and thus in the value of the directivity function and p_{max}. Also, for larger a_1/λ_1, changes in h/λ_1 or ℓ/a_1 which accompany changes in Θ_1 produce larger changes in the directivity function and thus in p_{max}.

Let the fields with p,s=0 be in the far field for $p > p_{far}$. From the condition given in eqn. (34) it can be shown that p_{far} increases with increasing a_1/λ_1 and decreasing h/λ_1 or ℓ/a_1. Also as discussed above p_{max} increases with increasing a_1/λ_1 and ℓ/a_1, but with decreasing h/λ_1. The results show that always $p_{max} > p_{far}$ for the range of parameters considered in Fig. 5. Notice that for decreasing ℓ/a_1, p_{max} decreases and p_{far} increases. Thus it is expected that for sufficiently small ℓ/a_1, $p_{max} < p_{far}$. But this does not happen for $\ell/a_1 \geq 2$.

It can also be shown that Θ_1 for the fields with p_{max}, which is denoted by $(\Theta_1)_{max}$, is in the main lobe of the directivity function for all the cases considered in Fig. 5.

2. Similar observations as for Fig. 5 can be made for Fig. 6. The conditions for Figs. 6 (a), (b), and (c) are the same as for Fig. 5 (a), (b), and (c), respectively, except the receiver is such that $a_2/a_1 = 1$ instead of a point receiver. It is observed from Figs. 5 and 6 that p_{max} tends to increase for $a_2/a_1 = 1$ compared with $a_2/a_1 = 0$.

For $a_2/a_1 > 0$, the complex frequency response $H_{p,0}$ is integrated over the receiving transducer contact area to find $\bar{H}_{p,0}$ and then $|\bar{H}_{p,0}|$. Suppose

$\overline{|H_{p,0}|}$ is the average of $|H_{p,0}|$ over the receiving transducer contact area. Also, suppose that $|H_{p,0}|_0$ is the value of $|H_{p,0}|$ evaluated at the center of the receiving transducer. For $\overline{|H_{p,0}|} \approx |H_{p,0}|_0$, which can be justified for the fields with Θ_1 in the main lobe, $|\overline{H}_{p,0}| \leq |H_{p,0}|_0$ if there is a change in the phase of $H_{p,0}$ over the averaging area. It can be shown that for smaller p the phase changes more over the receiving transducer contact area by considering that the imaginary point in M_p in Fig. 3 (b) is located at a smaller distance and at a larger angle from the source, and thus $|\overline{H}_{p,0}|$ decreases more compared with $|H_{p,0}|$. So, p_{max} tends to increase for $a_2/a_1 = 1$.

3. The conditions for Fig. 7 are the same as for Fig. 5 (b) except $\alpha_1\lambda_1$ is 0.005 and 0.01 in Figs. 7 (a) and (b), respectively, instead of lossless material. As observed from these plots, p_{max} decreases with increasing $\alpha_1\lambda_1$. The plots with attenuation show irregularities for large h/λ_1 and ℓ/a_1, where p_{max} does not necessarily decrease with increasing h/λ_1 or decreasing ℓ/a_1 as in lossless material. The regions with irregularities move towards smaller h/λ_1 or ℓ/a_1 with increasing $\alpha_1\lambda_1$.

As assumed in Sec. 6, $|H_{p,0}|$ decreases exponentially with the product of the attenuation constant and the distance of the imaginary point M_p from the origin in Fig. 3 (b). Thus, $|H_{p,0}|$ with larger p decreases more with increasing $\alpha_1\lambda_1$. So, p_{max} tends to become smaller with increasing $\alpha_1\lambda_1$.

Although $(\Theta_1)_{max}$ for the field with p_{max} is in the main lobe of the directivity function for $\alpha_1\lambda_1 = 0$ in Fig. 5 (b), it may jump to the side lobes for sufficiently large h/λ_1, ℓ/λ_1, and $\alpha_1\lambda_1$, and irregularities appear as in Fig. 7. While attenuation pushes p_{max} down, namely $(\Theta_1)_{max}$ up, $(\Theta_1)_{max}$ approaches to the critical angles where the directivity function is exactly

zero. Near these angles there are sharp changes in $|H_{p,0}|$ and thus p_{max} jumps to bigger or smaller values.

4. The conditions for Fig. 6 (b), 8 (a) and (b) are the same as for Fig. 5 (b), 7 (a) and (b), respectively, except $a_2/a_1 = 1$ instead of a point receiver.

For $a_2/a_1 = 1$, p_{max} decreases with increasing $\propto_1 \lambda_1$ again but the irregularities appeared for a point receiver do not exsist any more. This is because $|H_{p,0}|$ is not exactly zero near the critical angles due to the averaging over the receiving transducer contact area and there are no sharp changes.

5. Overall, Figs. 5-8 suggest that larger h/λ_1, smaller a_1/λ_1, and for attenuating material larger a_2/a_1 increase the stability of the output in the SWF configuration in terms of the reflection with the maximum magnitude. The stability means small changes in parameters produce small changes in the output.

8 CONCLUSIONS AND RECOMMENDATIONS

Steady-state harmonic stress waves in an isotropic elastic plate excited on one face by a circular transducer were analyzed theoretically. It was assumed that the transmitting transducer transforms an electrical voltage into a uniform normal stress at the top face of the plate. First, the radiation into a half- space, which introduced longitudinal (P) and shear (S) waves into the plate, and then their successive reflections at the bottom and top faces of the plate were considered to satisfy the boundary conditions.

A separate circular receiving transducer, also located at the top face of the plate, was considered. It was assumed that the receiving transducer produced an electrical voltage proportional to the average spatially integrated normal stress over its face due to an incident wave.

The frequency response at a receiving point due to a multiply reflected wave was formulated in integral form and its asymptotic behavior was given. The far field condition for the asymptotic solution to be valid was also discussed. This condition suggested that although the thickness of the plate may be small, the waves which reflect sufficiently many times satisfy the far field condition.

A numerical procedure was given to evaluate the frequency response at a receiving point due to a multiply reflected wave in the near field. Its stability and convergence were discussed. Also, exponential decay was introduced to account the material attenuation.

Calculations were done for aluminum plates. It was found that the numerical procedure becomes unstable for $h/\lambda_1 < 1.6$ where h is the thickness of the plate and λ_1 is the P wavelength.

Parametrized plots which determine the particular wave whose frequency response has maximum magnitude compared with other multiply reflected waves were given for a range of values of dimensionless parameters in the analysis. The effects of changes in the values of the parameters were discussed.

This study is part of an overall effort to develop quantitative analyses of ultrasonic nondestructive evaluation parameters such as the stress wave factor (SWF). The spectral analysis of the SWF signal should benefit from this study. The parametrized plots given in this study or generated using the results of this study may be used to estimate some parameters such as the material attenuation or the effective radius of the transmitting transducer from the spectral analysis of the SWF signal in terms of individual reflections.

Finally, stress wave transmission characteristics of plates in the SWF configuration should be analyzed using the modal analysis (Rayleigh- Lamb frequency spectrum) for small values of h/λ_1 where the numerical procedure given in this study becomes unstable.

REFERENCES

[1] A. Vary and R.F. Lark, "Correlation of Fiber Composite Tensile Strength with the Ultrasonic Stress Wave Factor", Journal of Testing and Evaluation, Vol. 7, No. 4, July 1979, pp. 185- 191.

[2] A. Vary and K.J. Bowles, "An Ultasonic- Acoustic Technique for Nondestructive Evaluation of Fiber Composite Quality", Polymer Engineering and Science, Vol. 19, No. 5, April 1979, pp. 373-376.

[3] J.H. Williams, Jr., and N.R. Lampert, "Ultrasonic Evaluation of Impact- Damaged Graphite Fiber Composite", Materials Evaluation, Vol. 38, No. 12, December 1980, pp. 68-72.

[4] J.H. Williams, Jr., and B. Doll, "Ultrasonic Attenuation as an Indicator of Fatique Life of Graphite Fiber Epoxy Composites", Materials Evaluation, Vol. 38, No. 5, May 1980, pp. 33- 37.

[5] J.H. Williams, Jr., H. Yuce, and S.S. Lee, "Ultrasonic and Mechanical Characterizations of Fatique States Of Graphite Epoxy Composite Laminates", Materials Evaluation, Vol. 40, No. 5, April 1982, pp. 560- 565.

[6] J. Krautkramer and H. Krautkramer, Ultrasonic Testing of Materials, Second Edition, Springer- Verlag, Inc.,N.Y., 1977.

[7] J.H. Williams,Jr., H. Karagulle, and S.S. Lee, "Ultrasonic Input-Output for Transmitting and Receiving Longitudinal Transducers Coupled to Same Face of Isotropic Elastic Plate", Materials Evaluation, Vol. 40, No. 6, May 1982, pp. 655-662.

[8] G.F. Miller and H. Pursey, "The Field and Radiation Impedance of Mechanical Radiators on the Free Surface of a Semi-infinite Isotropic Solid", Proceedings of the Royal Society of London, Series A, Vol. 223, May 1954, pp. 521-541.

[9] W.J. Pardee, "Radially Propogating Surface and Plate Waves", J. Acoust. Soc. Am., Vol.71, No.1, January 1982, pp. 1-4.

[10] Y.H. Pao, R.R. Gajewski, "The Generalized Ray Theory and Transient Responses of Layered Elastic Solids", Physical Acoustics,Vol. XIII, Ed. by W.P. Mason and R.N. Thurston, Academic Press, N.Y., 1977, pp. 183-265.

[11] A.N. Ceranoglu and Y.H. Pao, "Propogation of Elastic Pulses and Acoustic Emission in a Plate", Parts 1-3, Journal of Applied Mechanics, Vol. 48, No. 1, March 1981, pp. 125-147.

[12] K.F. Graff, Wave Motion in Elastic Solids, The Ohio State University Press, Columbus, OH, 1975.

[13] H. Karagulle, "Ultrasonic Input- Output for Transmitting and Receiving

Transducers Coupled to Same Face of Isotropic Elastic Plate", Composite Materials and Nondestructive Evaluation Laboratory, Massachusetts Institute of Technology, Cambridge, Mass., Unpublished Report, 1984.

[14] T.W. Spencer, "The Method of Generalized Reflection and Transmission Coefficients", Geophysics, Vol. 25, No. 3, June 1960, pp. 625- 641.

[15] S.A. Orszag, Advanced Mathematical Methods for Scientists and Engineers, McGraw Hill, Inc., N.Y., 1978.

[16] R.W. Hornbeck, Numerical Methods, Prentice Hall, Inc., Englewood Cliffs, N.J., 1975.

[17] P.M. Morse and K.M. Ingard, Theoretical Acoustics, McGraw Hill, Inc., N.Y., 1968.

[18] R.B. Lindsay, Mechanical Radiation, McGraw Hill, Inc., N.Y., 1960.

[19] F.B. Hildebrand, Advanced Calculus for Applications, Prentice- Hall, Inc., Englewood Cliffs, N.J., 1962.

[20] I. Tolstoy, Wave Propogation, McGraw Hill, Inc., N.Y., 1973.

[21] R.W. Bracewell, The Fourier Transform and Its Applications, McGraw Hill, Inc., N.Y., 1965.

[22] A.V. Oppenheim and R.W. Schafer, Digital Signal Processing, Prentice-Hall, Inc., Englewood Cliffs, N.J., 1975

[23] H. Karagulle, J.H. Williams, Jr., and S.S. Lee, "Application of Homomorphic Signal Processing to Stress Wave Factor Analysis", Composite Materials and Nondestructive Evaluation Laboratory, Massachusetts Institute of Technology, Cambridge, Mass., Report Under Preparation.

[24] G.L. Gooberman, Ultrasonics— Theory and Application, Hart Publishing Company, N.Y., 1968.

TABLE 1 Displacements[a] and Stresses[a] in Isotropic Elastic Solid with Axial Symmetry and Zero Rotational Displacement [12].

	From Longitudinal Wave Potential Φ[b]	From Shear Wave Potential ψ
u_r	$\dfrac{\partial \Phi}{\partial r}$	$\dfrac{\partial^2 \psi}{\partial r\, \partial z}$
u_z	$\dfrac{\partial \Phi}{\partial z}$	$\dfrac{\partial^2 \psi}{\partial z^2} - \dfrac{1}{c_2^2}\dfrac{\partial^2 \psi}{\partial t^2}$
u_ϕ	0	0
σ_{rr}	$\dfrac{\lambda}{c_1^2}\dfrac{\partial^2 \Phi}{\partial t^2} + 2\mu\dfrac{\partial^2 \Phi}{\partial r^2}$	$2\mu\dfrac{\partial^3 \psi}{\partial r^2\, \partial z}$
σ_{zz}	$\dfrac{\lambda}{c_1^2}\dfrac{\partial^2 \Phi}{\partial t^2} + 2\mu\dfrac{\partial^2 \Phi}{\partial z^2}$	$2\mu\dfrac{\partial}{\partial z}\left(\dfrac{\partial^2 \psi}{\partial z^2} - \dfrac{1}{c_2^2}\dfrac{\partial^2 \psi}{\partial t^2}\right)$
$\sigma_{\phi\phi}$	$\dfrac{\lambda}{c_1^2}\dfrac{\partial^2 \Phi}{\partial t^2} + \dfrac{2\mu}{r}\dfrac{\partial \Phi}{\partial r}$	$\dfrac{2\mu}{r}\dfrac{\partial^2 \psi}{\partial r\, \partial z}$
σ_{rz}	$2\mu\dfrac{\partial^2 \Phi}{\partial r\, \partial z}$	$\mu\dfrac{\partial}{\partial r}\left(2\dfrac{\partial^2 \psi}{\partial z^2} - \dfrac{1}{c_2^2}\dfrac{\partial^2 \psi}{\partial t^2}\right)$
$\sigma_{r\phi}$	0	0
$\sigma_{z\phi}$	0	0

a u_r, u_z, u_ϕ are the components of the displacement vector, and $\sigma_{rr}, \sigma_{zz}, \sigma_{\phi\phi}, \sigma_{rz}, \sigma_{r\phi}, \sigma_{z\phi}$ are the components of the stress tensor in the cylindrical coordinates.

b λ and μ are Lame' constants.

TABLE 2 Calculated Values of K_F for Analog Acoustics
        Problem.

a/λ_0	K_F	
	For $E_a = 5\%$	For $E_a = 3\%$
0.2	11.4	18.2
0.4	6.2	10.0
1.0	3.8	5.8
2.0	3.2	5.0
3.0	3.2	4.8
4.0	3.0	4.8
5.0	3.0	4.8
7.0	3.0	4.6
10.0	3.0	4.6

TABLE 3 Subintervals and Corresponding Numerical Integration Methods Used to Evaluate the Integral in Eqn. (18).

Subinterval		Numerical Integration Method
From	To	
0	$1-\epsilon^a$	Trapezoidal[b]
$1-\epsilon$	1	Gauss[c]
1	$1+\epsilon$	"
$1+\epsilon$	$k-\epsilon$	Trapezoidal
$k-\epsilon$	k	Gauss
k	ξ_R	"
ξ_R	$\xi_1=\xi_R+\epsilon$	"
ξ_1	$\xi_2=\xi_1+\xi_{inc}^d$	Trapezoidal
ξ_2	$\xi_3=\xi_2+\xi_{inc}$	"
$\vdots$	$\vdots$	"
ξ_{k-1}	$\xi_k=\xi_{k-1}+\xi_{inc}$	"
ξ_k^e	∞	Neglected

a $\epsilon\ll1$, typically $\epsilon=0.01$.

b Number of steps is increased by powers of 2 and the convergence is checked. When the integral converges to a value with an acceptable error, typically to within of 0.001, the integration is stopped.

c Typically 8 point Gauss-Legendre quadrature is used.

d Typically, $\xi_{inc}=1$.

e The integration is stopped at ξ_k when the integral over the interval from ξ_{k-1} to ξ_k becomes negligibly small, typically smaller than 0.001.

$$\sigma_{zz} = \begin{cases} e^{-iwt} & \text{for} \quad 0 \le r \le a_1 \\ 0 & \text{for} \quad r > a_1 \end{cases}$$

(a)

(b)
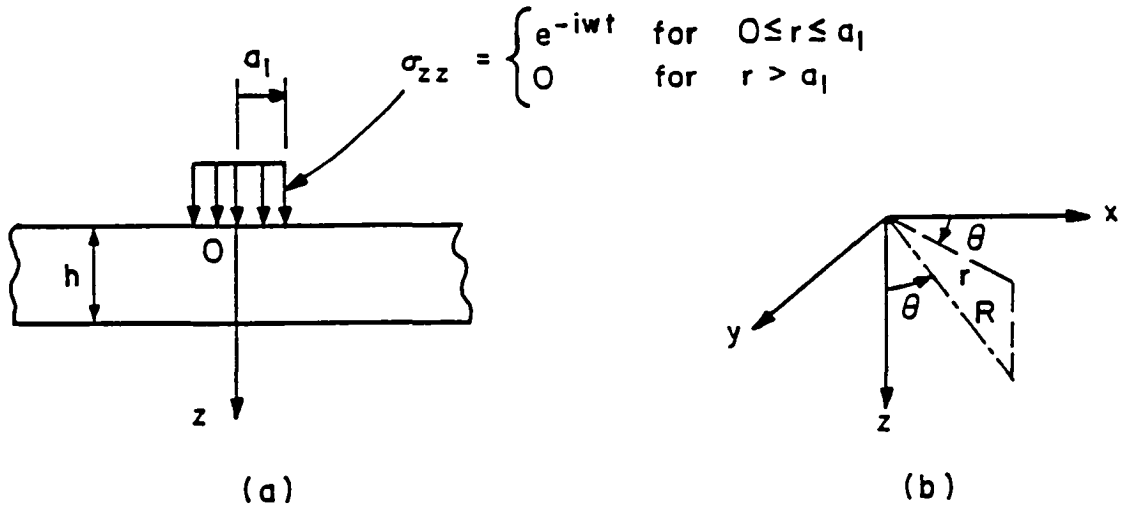
Fig. 1 Schematics of (a) plate with axially symmetric excitation and (b) coordinate systems.

Stage	Waves	Boundary Conditions Satisfied Only at
1	P S	z = 0
2	P S P S	z = h
3	P S P S P S P S	z = 0
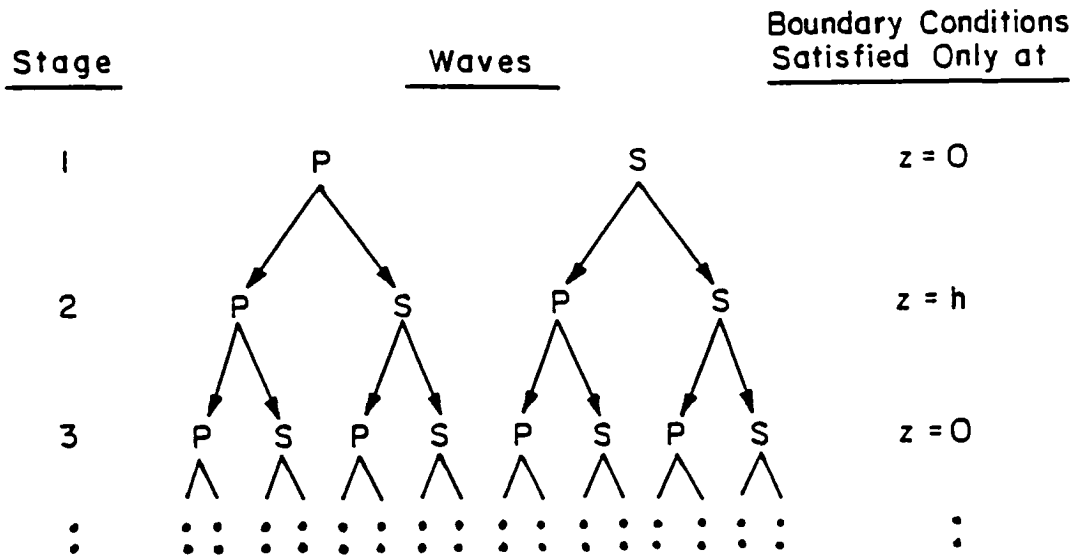
Fig. 2 Representation of introducing reflected waves at successive stages as binary tree.

$$\sin \theta_1 = k \sin \theta_2$$

(a)

(b)
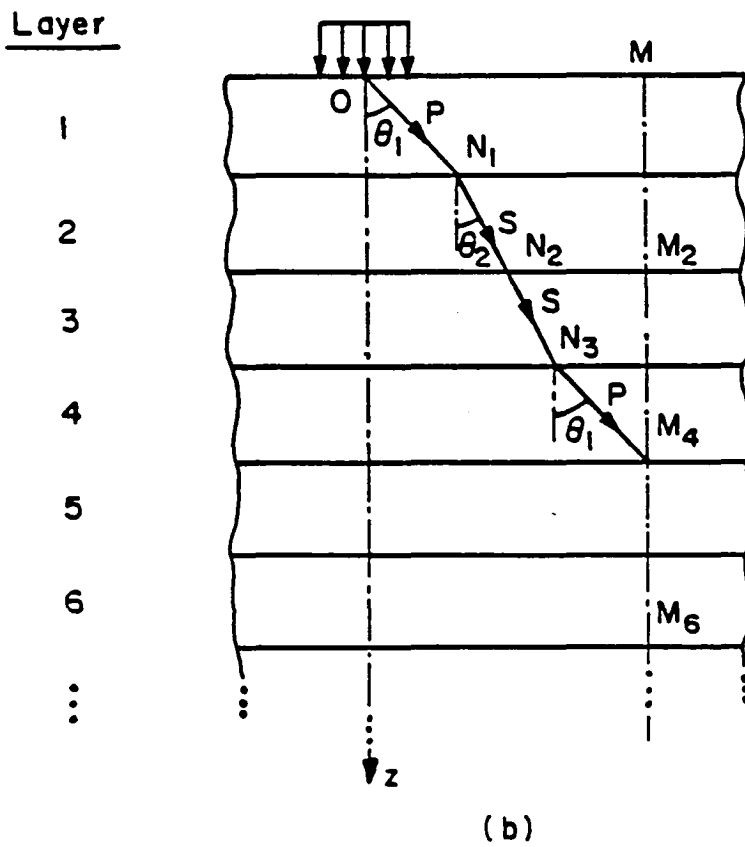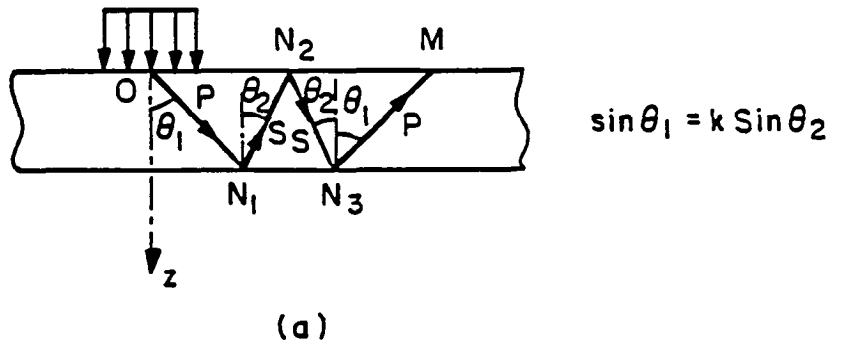
Fig. 3 Schematics of (a) plate and the PSSP ray and (b) hypothetical
multi-layered half-space and the PSSP ray.
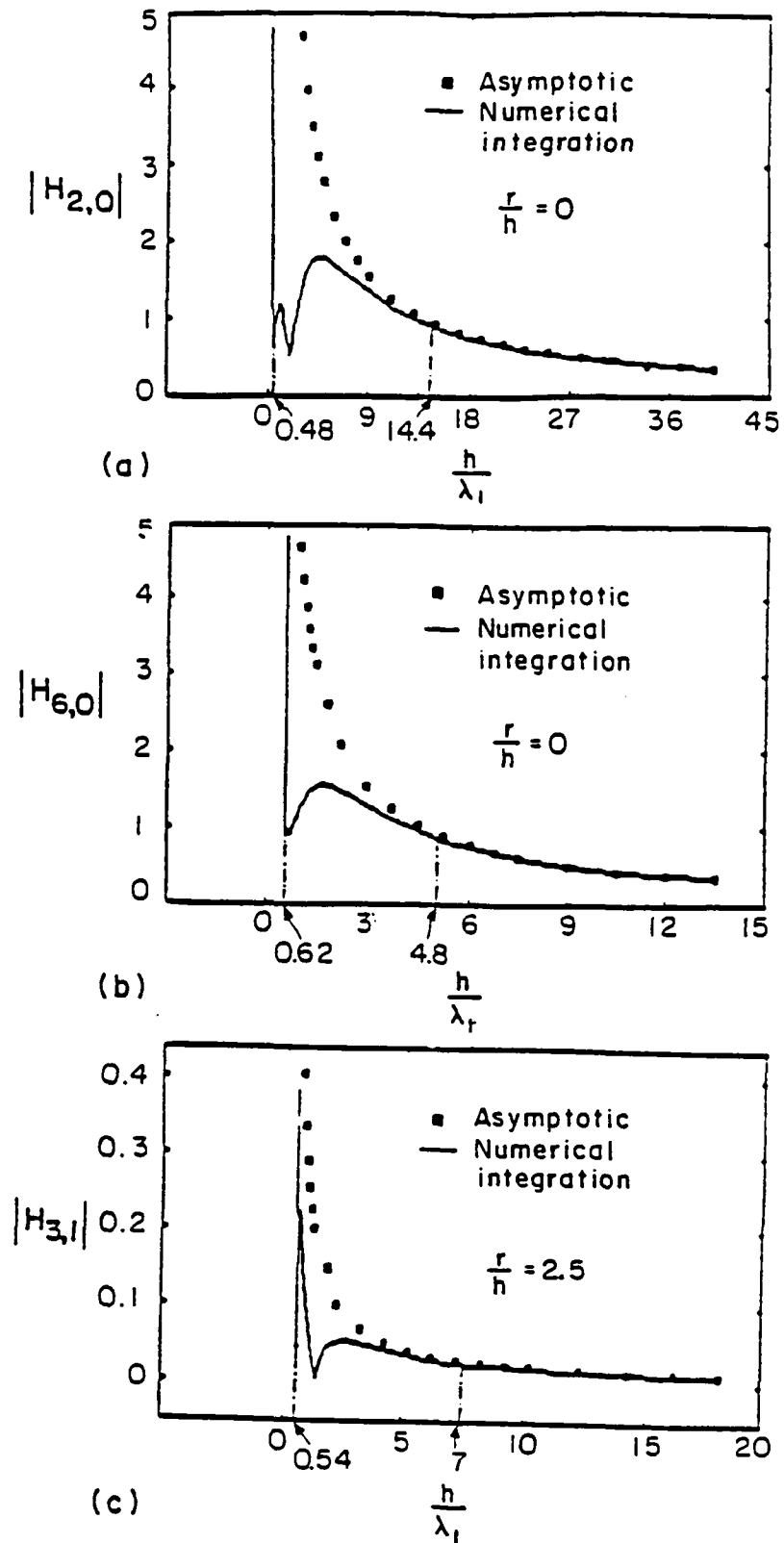
Fig. 4 Behavior of (a) $|H_{2,0}|$, (b) $|H_{6,0}|$, (c) $|H_{3,1}|$ versus h/λ_1 for $k=2.02$, $a_1/\lambda_1=3$.
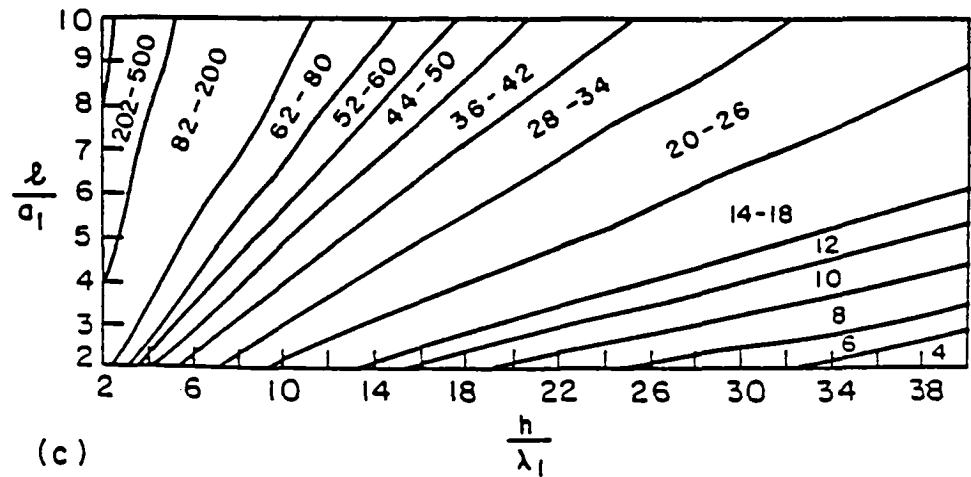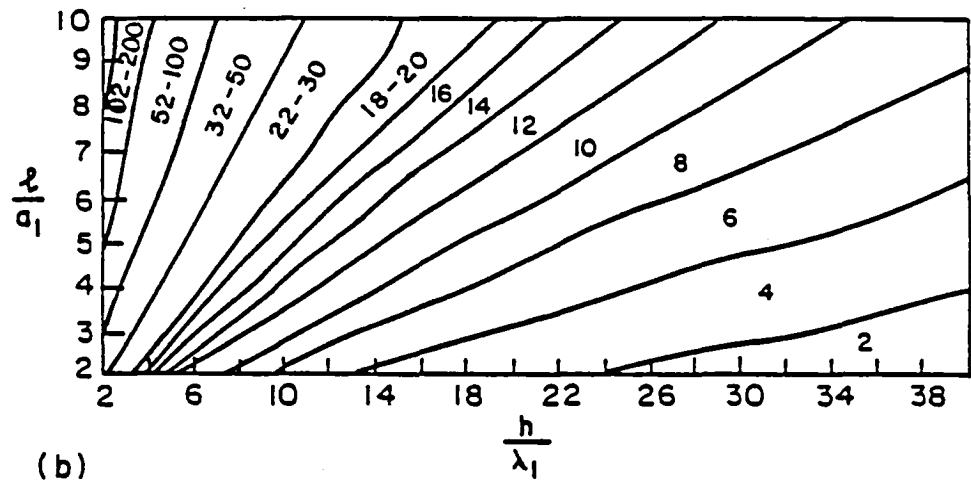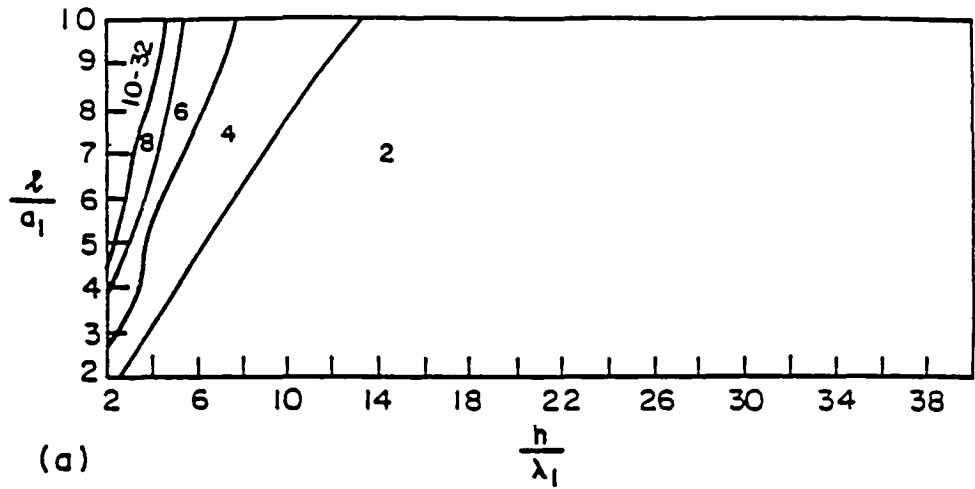
Fig. 5 Parametrized plots for $k=2.02$, $\alpha_1 \lambda_1 = 0$, $s=0$, $a_2/a_1 = 0$ (point receiver) and (a) $a_1/\lambda_1 = 1$, (b) $a_1/\lambda_1 = 3$, and (c) $a_1/\lambda_1 = 5$.
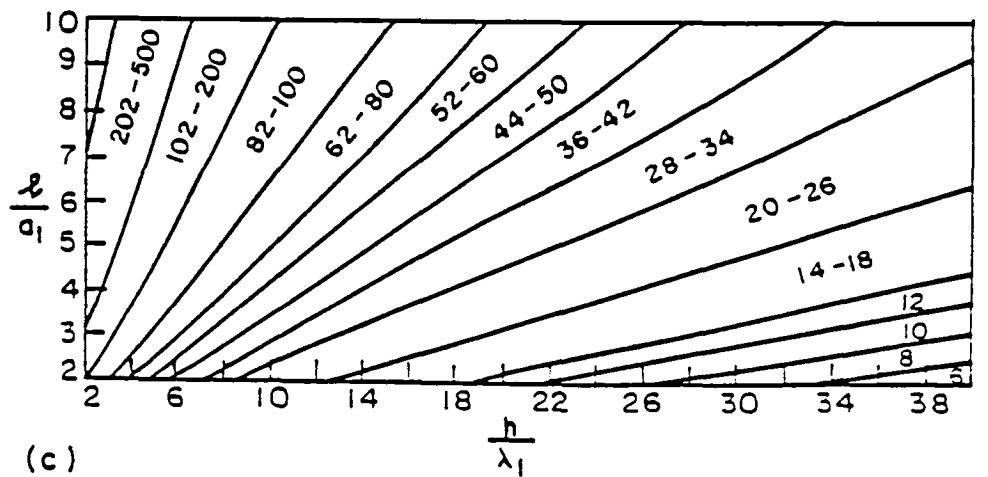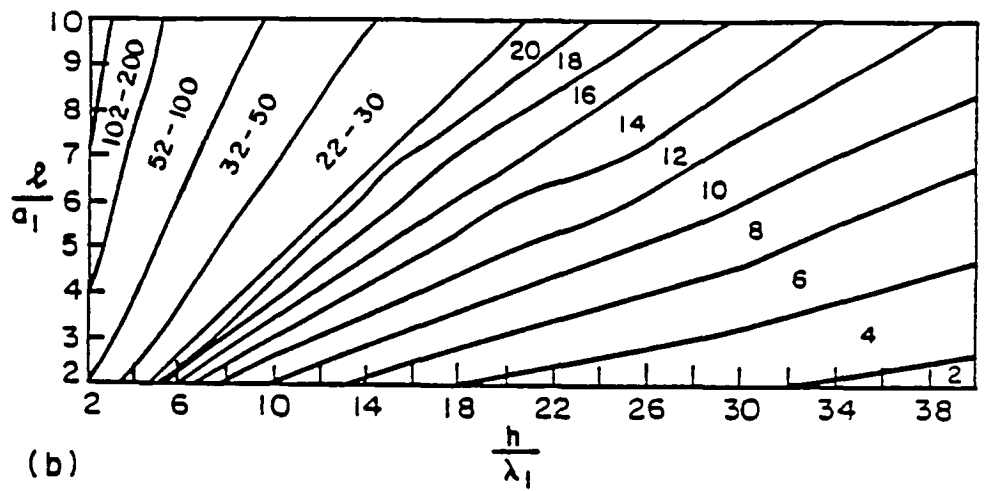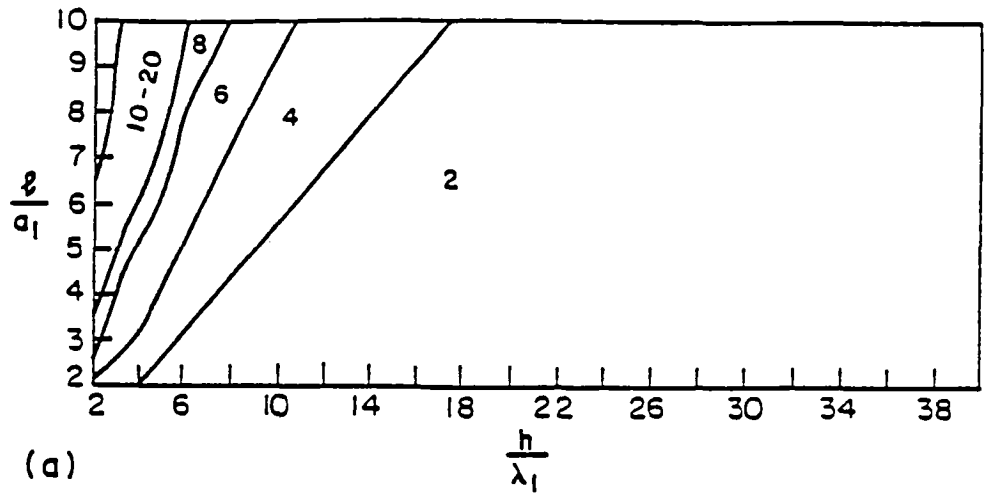
Fig. 6 Parametrized plots for k=2.02, $\alpha_1\lambda_1=0$, s=0, $a_2/a_1=1$ and (a) $a_1/\lambda_1=1$, (b) $a_1/\lambda_1=3$, and (c) $a_1/\lambda_1=5$.
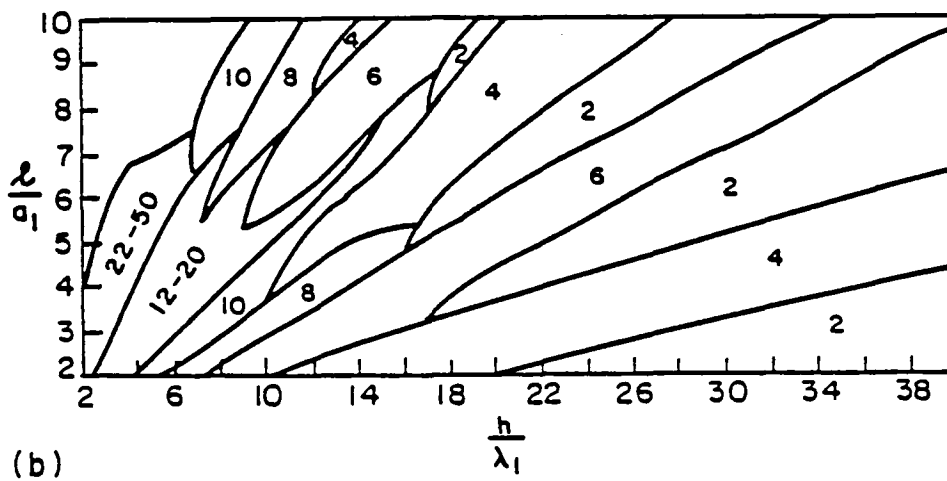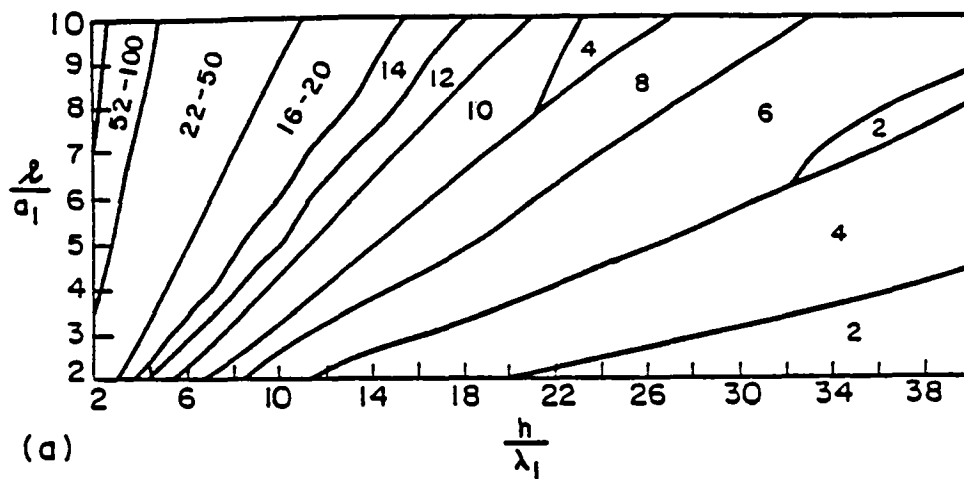
(a)

(b)

Fig. 7 Parametrized plots for k=2.02. (a) $\alpha_1 \lambda_1 = 0.005$, and (b) $\alpha_1 \lambda_1 = 0.01$, and s=0, $a_2/a_1 = 0$ (point receiver), $a_1/\lambda_1 = 3$.
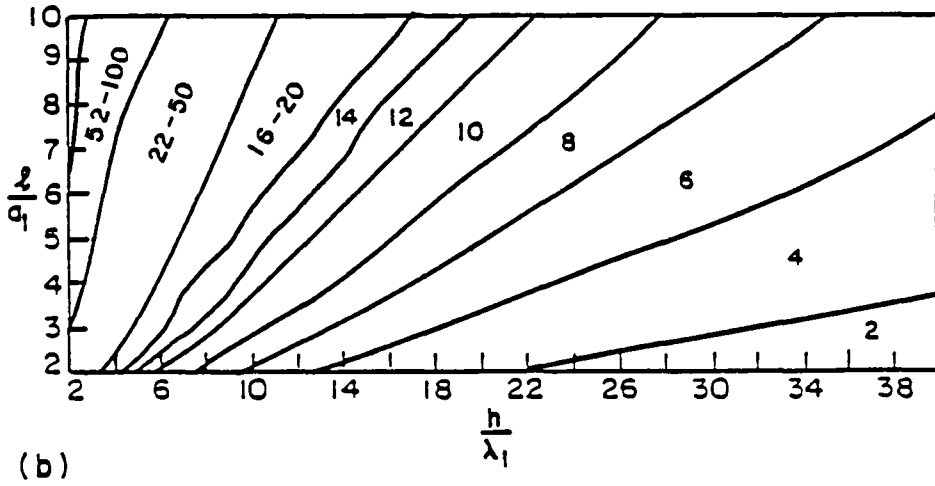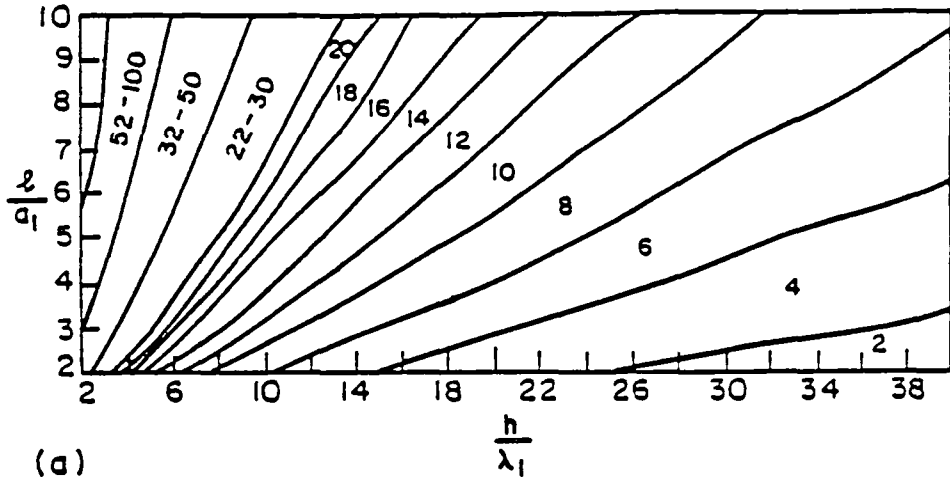
(a)

(b)

Fig. 8 Parametrized plots for k=2.02. (a) $\alpha_1 \lambda_1 = 0.005$, and (b) $\alpha_1 \lambda_1 = 0.01$, and s=0, $a_2/a_1 = 1$, $a_1/\lambda_1 = 3$.

1. Report No. NASA CR-3877	2. Government Accession No.	3. Recipient's Catalog No.
4. Title and Subtitle Stress Waves in an Isotropic Elastic Plate Excited by a Circular Transducer		5. Report Date March 1985
		6. Performing Organization Code
7. Author(s) Hira Karagulle, James H. Williams, Jr., and Samson S. Lee		8. Performing Organization Report No. None
		10. Work Unit No.
9. Performing Organization Name and Address Massachusetts Institute of Technology Department of Mechanical Engineering Cambridge, Massachusetts 02139		11. Contract or Grant No. NAG3-328
12. Sponsoring Agency Name and Address National Aeronautics and Space Administration Washington, D.C. 20546		13. Type of Report and Period Covered Contractor Report
		14. Sponsoring Agency Code 506-53-1A (E-2436)

15. Supplementary Notes

Final report. Project Manager, Alex Vary, Structures Division, NASA Lewis Research Center, Cleveland, Ohio 44135.

16. Abstract

Steady-state harmonic stress waves in an isotropic elastic plate excited on one face by a circular transducer are analyzed theoretically. It is assumed that the transmitting transducer transforms an electrical voltage into a uniform normal stress at the top face of the plate. To solve the boundary value problem, first the radiation into a half-space is considered. This introduces longitudinal (P) and shear (S) waves into the plate. Then, reflections are considered successively at the bottom and top faces of the plate. Each reflection produces both P and S waves for each incident P or S wave. A separate circular receiving transducer, also located at the top face of the plate, is considered. It is assumed that the receiving transducer produces an electrical voltage proportional to the average spatially integrated normal stress over its face due to an incident wave. The asymptotic behavior of the frequency response at a receiving point due to a multiply reflected wave is given. It is found that a receiving point observes an incident wave asymptotically as a plane wave which propagates and reflects in the direction of the multiply reflected ray constructed geometrically using Snell's law. The far field condition, for which the asymptotic solution is valid, is also discussed. This condition suggests that although the thickness of the plate may be small, the waves which reflect sufficiently many times do satisfy the far field condition. A numerical procedure is given to evaluate the frequency response at a receiving point due to a multiply reflected wave in the near field. Its stability and convergence are discussed. Also, exponential decay is introduced to account for material attenuation. Calculations are done for aluminum plates. It is found that the numerical procedure becomes unstable for $h/\lambda_1 < 1.6$ where h is the thickness of the plate and λ_1 is the P wavelength. Parameterized plots which determine the particular wave whose frequency response has maximum magnitude compared with other multiple reflected waves are given for a range of values of dimensionless parameters. The effects of changes in the values of the parameters are discussed.

17. Key Words (Suggested by Author(s)) Ultrasonics; Nondestructive testing; Elastic waves; Stress waves; Shear waves; Longitudinal waves; Harmonic wave analysis	18. Distribution Statement Unclassified - Unlimited STAR Category 38	
19. Security Classif. (of this report) Unclassified	20. Security Classif. (of this page) Unclassified	21. No. of pages 51	22. Price* A04

National Aeronautics and
Space Administration

Washington, D.C.
20546

THIRD-CLASS BULK RATE

Postage and Fees Paid
National Aeronautics and
Space Administration
NASA-451

U.S.MAIL

NASA

POSTMASTER: If Undeliverable (Section 158
Postal Manual) Do Not Return